Biochemical Pharmacology 82 (2011) 1510–1520

Contents lists available at ScienceDirect

Biochemical Pharmacology

journal homepage: www.elsevier.com/locate/biochempharm

Heteroplasmic mitochondrial disease in *Dictyostelium discoideum*

Lisa M. Francione, Paul R. Fisher *

Department of Microbiology, La Trobe University, VIC 3086, Australia

ARTICLE INFO

Article history:
Received 22 May 2011
Accepted 6 July 2011
Available online 20 July 2011

Keywords:
Dictyostelium
Phototaxis
Cell growth
Legionella
Mitochondrial disease

ABSTRACT

The bewildering complexity of the relationship between genotype and phenotype in human mitochondrial diseases has delayed an understanding of the related cytopathological mechanisms. To explore the relationship between mitochondrial dysfunction in *Dictyostelium discoideum* and the related cytopathologies, we determined whether the phenotypic outcomes were similar regardless of which *D. discoideum* mitochondrial gene was targeted for disruption. The disruption of the mitochondrial genes resulted in a similar pattern of phenotypes to those caused by other mitochondrial defects. These include impairment of phototaxis, multicellular development and growth on plates and in liquid medium. As the reduced growth rates could have been due to defective phagocytic or macropinocytic nutrient uptake, these processes were tested but found to be unaffected. Since mitochondria have been associated with *Legionella* pathogenesis of human macrophages, it was also determined if mitochondrially diseased *Dictyostelium* strains were better or worse than healthy cells at supporting the growth of *Legionella pneumophila*. The results revealed that the mitochondrially diseased strains supported greater *L. pneumophila* growth than the wild type *Dictyostelium* strain (AX2). Quantitative Northern blotting showed a significant reduction in the level of expression of the entire mitochondrial genome, regardless of which mitochondrial gene was targeted for disruption, suggesting a generalized deficiency in mitochondrial gene expression and function. The phenotypic outcomes were the same as those shown previously to result from chronic hyperactivity of the energy-sensing protein kinase, AMPK, after knockdown of mitochondrial chaperonin 60.

1. Introduction

Mutations in mitochondrial or nuclear genes that encode essential mitochondrial proteins are associated with an array of human mitochondrial diseases. Unfortunately the complexities of mammalian developmental and mitochondrial biology have meant that the clinical outcomes of mitochondrial disease are not predictable from the genetic defect causing them. Individuals with the same mutation can exhibit very different signs and symptoms while different genetic defects can cause very similar pathologies. Depending on which tissues are affected most in a given individual, this leads to a bewildering complexity in mitochondrial diseases which exhibit a very broad range of possible symptoms. These symptoms can include epilepsy, stroke-like episodes, muscle weakness, ataxia, exercise intolerance, parkinsonism, blindness, deafness, diabetes, kidney malfunction, heart conditions and various combinations of these clinical manifestations [1–4]. Examples of mitochondrial diseases include Myoclonic Epilepsy with Ragged-Red Fibers (MERRF); Mitochondrial Encephalomyopathy, Lactic Acidosis and Stroke-like episodes (MELAS); Leber's Hereditary Optic Neuropathy (LHON); Neuropathy, Ataxia and Retinitis Pigmentosa (NARP); and Leigh syndrome (LS) [1,4].

To effectively treat mitochondrial diseases a clear understanding of the associated disease mechanisms is necessary. In recent years *Dictyostelium* has emerged as a valuable model organism to investigate the molecular basis for cytopathologies associated with mitochondrial dysfunction [5–13]. An advantage of the *Dictyostelium* model is that it offers a tractable microbial system in which a wide range of readily assayed, reproducible phenotypes can been studied. In mitochondrial disease studies these have included phototaxis, thermotaxis, chemotaxis, growth in suspension and on bacterial lawns, phagocytosis, macropinocytosis, multicellular morphogenesis and susceptibility to the intracellular bacterial pathogen *Legionella pneumophila* [7,9]. Each of these phenotypes is the endpoint of regulatory signal transduction pathways whose functions may be disturbed as a result of mitochondrial dysfunction. Indeed it was proposed in the earliest studies that the primary cytopathological effect of mitochondrial disease in *D. discoideum* is dysregulation of cellular signal transduction pathways [11,13].

We previously generated mitochondrial dysfunction either by disruption of the large rRNA subunit gene (*rnl*) in a subset of the

* Corresponding author. Tel.: +61 3 9479 2229; fax: +61 3 9479 1222.
E-mail addresses: L.Francione@latrobe.edu.au (L.M. Francione), P.Fisher@latrobe.edu.au (P.R. Fisher).

0006-2952/$ – see front matter © 2011 Elsevier Inc. All rights reserved.
doi:10.1016/j.bcp.2011.07.071

mitochondrial genomes (a state referred to as heteroplasmy) [13] or by antisense inhibition of expression of chaperonin 60, an essential nuclear-encoded mitochondrial protein [11]. The former would impair protein synthesis in the subpopulation of mitochondria in which *rnl* was disrupted, while the latter would reduce the protein-folding capacity of the mitochondria. In both cases, photo- and thermotaxis, growth in liquid medium and multicellular development were impaired, prompting the suggestion that the phenotypic outcomes of mitochondrial dysfunction in *Dictyostelium* are the same, regardless of the underlying genetic cause. In the work reported here, we test this hypothesis further by examining the phenotypic consequences of heteroplasmic disruption of eight further mitochondrial genes distributed around the mitochondrial genome [14]. These genes included some that encode subunits of respiratory chain enzymes, *atp1*, *atp6*, *cob*, *cox3*, *nad2* and *nad5*, as well as the open reading frames *ORF1740* and *ORF796*. *ORF1740* encodes a ribosomal protein, S3 C-terminal domain-containing protein, whereas the function of the *ORF796* product is unknown.

After the original studies of mitochondrial dysfunction in *Dictyostelium*, a wider range of phenotypes was investigated in chaperonin 60 antisense-inhibited strains [7,9] and in knockout mutants lacking a novel mitochondrial protein, MidA [12,15]. Some phenotypes were common to both kinds of mutant, namely defective phototaxis, thermotaxis, growth in suspension and on plates. However the chaperonin 60 antisense-inhibited strains exhibited normal phagocytosis and macropinocytosis rates [7], while the *midA*$^{-}$ mutant was defective for both of these phenotypes [12]. Here we show that the phenotypic outcomes of disrupting any of 9 different mitochondrial genes are similar to those arising from chaperonin 60 antisense inhibition and different from those reported in the *midA* knockout mutant.

The *Dictyostelium* mitochondrial genome is transcribed unidirectionally from a single promoter and the transcript is processed to produce the mature RNA products [16]. We show here that regardless of which gene is targeted, heteroplasmic mitochondrial gene disruption causes a coordinate reduction in expression of transcripts encoded near the start, middle and end of the primary transcript i.e. expression of the entire mitochondrial genome is depressed. This generalized mitochondrial dysfunction contrasts with the specific impairment of Complex I activity observed when MidA is knocked out [15], but is akin to the general effects on mitochondrial protein synthesis or folding expected in *rnl* disruptants or chaperonin 60 knockdown strains.

2. Methods

2.1. Plasmid constructs and Dictyostelium strains

All experiments were performed with *D. discoideum* parental strain AX2 [30] and mutants created from it. *D. discoideum* mutant strains were created by heteroplasmic disruption of nine mitochondrial genes using the previously described strategy [13]. The approach is based on homologous recombination between the mitochondrial genome and a circular plasmid molecule containing an insert of 500–1000 bp of the targeted gene. Cells were transformed with the circular plasmid construct and stable transformants were selected on the basis of G418 [geneticin (Promega Corporation, Annandale, NSW, Australia)] resistance expressed under the control of a constitutive chromosomal gene promoter in the vector. The desired, targeted insertions into the mitochondrial genome are accompanied by multiple, independent insertions at nontargeted locations in the nuclear genome [13]. Each of these random chromosomal insertions contains scores to hundreds of tandemly duplicated copies of the construct that are produced by rolling circle replication during the insertion process [20]. In such targeted disruption experiments, the desired insertion into the targeted gene occurs only in a minority of transformants. In this work we therefore screened the transformants initially for mitochondrial gene disruptions on the basis of the phototaxis-deficient phenotype previously shown to be characteristic of mitochondrial dysfunction. This was followed by Southern blotting to verify the presence of plasmid insertions into the mitochondrial genome as previously [13] (see Section 3). The plasmid constructs and mutant strains isolated using them are listed in Table 3.

Chaperonin 60 antisense mutants (HPF406-418) were described previously by Kotsifas et al. [11]. The mitochondrial, large ribosomal RNA gene (*rnl*) mutants (HPF266–270) were described previously by Wilczynska et al. [13].

2.2. Culture conditions

Cells grown axenically were cultured in HL-5 liquid medium [30] supplemented with 100 μg/ml ampicillin (Roche Diagnostics Australia Pty. Ltd., Castle Hill, NSW Australia), 20 μg/ml streptomycin (Boehringer Mannheim Australia Pty. Ltd., Castle Hill, NSW Australia) and 10 μg/ml tetracycline (Sigma–Aldrich Pty. Ltd., Castle Hill, NSW Australia). Strains were also grown on bacterial lawns prepared from *Klebsiella aerogenes* on SM agar. As a selective marker, G418 (geneticin) (20 ug/ml) was added to the growth media for all transformants during subculturing. However, for phenotypic studies antibiotics were excluded from media to avoid any possible antibiotic-associated effects.

2.3. Phototaxis

A small quantity of amoebae was scraped from the edges of *Dictyostelium* colonies on *K. aerogenes* lawns by toothpick and transferred to non-nutrient charcoal agar plates [1.0% agar (Oxoid Australia Pty. Ltd., Adelaide, South Australia, Australia), 0.5% activated charcoal (Sigma–Aldrich)] [18,31]. After incubation with a lateral light source for 24–48 h, slugs and slime trails were transferred to clear polyvinyl chloride (PVC) discs. The discs were stained for 5 min with Coomassie blue (Sigma–Aldrich) [31] and rinsed gently with running tap water. To perform quantitative analysis, start and end points of the stained trails were digitised and stored as *x*, *y* coordinates through use of the Summagraphics 120 digitising tablet connected to a SUN workstation (SUN Microsystems, Santa Clara, CA, USA), and analysed using directional statistics based on the von Mises or circular normal distribution [18].

2.4. Pulsed field gel electrophoresis and Southern blot analysis

For PFGE the cells were prepared according to the method of Cox et al. [32]. The cells were washed twice in ice-cold phosphate buffer [17 mM Na/K phosphate (Ajax Chemicals Pty. Ltd., Auburn, NSW, Australia), pH 6.0] and then mixed with an equal volume of 2% InCert® low melting (LM) point agarose (FMC BioProducts, Rockland, ME, USA) which was precooled to 39 °C. The mixture (final density = (4–5) × 10^8 cells/ml) was then quickly pipetted into prewarmed moulds (~250 μl for each plug). The solidified plugs (~30 μl) were incubated in digestion buffer [0.5 M EDTA (Sigma–Aldrich), pH 8.0; 2% sodium lauroyl-sarcosinate (Sigma–Aldrich); 2 mg/ml Proteinase K (Gibco BRL, Gaithersburg, MD, USA)] for 48 h at 50 °C.

A series of washes were performed before restriction enzyme digestion of DNA. The agarose plugs were repeatedly washed in TE buffer containing 1 mM phenylmethylsulfonyl fluoride [PMSF (Sigma™)] to inactivate Proteinase K. The plugs were then repeatedly washed in TE for 30 min at RT to remove the PMSF and any remaining N-Lauroylsarcosine (Sigma–Aldrich). The

washed plugs were then incubated at 37 °C for ~14 h in a digestion mix containing 100 μl H_2O, 15 μl 10× restriction buffer and 5 μl of the restriction enzyme *Bln*I [50-100 U (Roche Diagnostics Australia)].

PFGE was conducted with a BioRad CHEF DR® II apparatus (Contour-clamped Homogenous Electric Fields; [33]). PFGE gels contained 1% (w/v) agarose (Promega Corporation) in 0.5× TBE running buffer. The PFGE conditions used were 60 s ramped switching time (60 s initial, 120 s final) at 200 V and 14 °C for 22 h. The gels were analysed through Southern blot hybridisation. Southern transfer was by acid depurination and alkaline transfer to nylon membranes [Hybond (Amersham Biosciences Ltd., Buckinghamshire, UK)]. The blots were hybridised with a DIG (Roche Diagnostics Australia)-labelled mtDNA probe or a radioactively-labelled pIC19H DIG-labelled probe.

2.5. Morphology

Multicellular development was examined after culturing transformants on *E. coli* B/2 lawns on SM agar plates. The SM agar plates were prepared by spreading 0.1 ml of a dense *Escherichia coli* B/2 suspension in sterile saline onto the surface of the plates and allowing the inoculum to dry in the laminar flow hood before streak inoculating amoebae of the transformants onto the lawns. The plates were incubated at 21 °C for 4–6 days to monitor growth and multicellular development.

2.6. Growth experiments

2.6.1. Growth on bacterial lawns

To determine growth rates on bacterial lawns a similar procedure to that used by Bokko et al. [7] was performed. *E. coli* B2 lawns were prepared on NA (NA: 20 g/L Bacto agar [Difco Laboratories Pty. Ltd., Detroit, MI, USA]; 1 g/l Bacto peptone (Oxoid Australia), 1.1 g/l anhydrous glucose, 1.9972 g/l KH_2PO_4 (Ajax Chemicals) and 0.356 g/l $Na_2HPO_4{\cdot}2H_2O$ (Ajax Chemicals), pH 6.0. 20 μl droplets of suspensions containing 1×10^6 *Dictyostelium* amoebae/ml were pipetted onto the centre of NA plates and incubated at 21 °C for 5 days. The diameter in mm of the resulting *D. discoideum* plaques was recorded at intervals of 8 or 12 h. The results were analysed by linear regression using the "R environment for statistical computing and graphics (http://www.R-project.org)" to determine the plaque expansion rate.

2.6.2. Growth in axenic medium

Dictyostelium cells growing exponentially in a 50 ml HL-5 culture were subcultured into fresh HL-5 medium at a density of 1×10^4 cells/ml and incubated at 21 °C with shaking at 150 rpm on an orbital shaker. The cell densities were observed using a haemocytometer at 8 or 12 h intervals over a period of 5 days. The cell densities were then analysed by log-linear regression using the R programming environment computer software to determine the generation time from the exponential growth curve. The 95% confidence intervals for the generation time were calculated from confidence intervals for the slope of the log-linear portion of the growth curve.

2.7. Phagocytosis

Phagocytosis was studied using a protocol previously described by Bokko et al. [7]. The bacteria ingested by *Dictyostelium* was an *E. coli* strain expressing a fluorescent protein termed DsRed (DsRed-Ec) [34]. This strain was prepared at a density of $(2–4) \times 10^{10}$ bac- bacteria/ml (equivalent to OD_{600} = 10–20) in 20 mM Sorenson's buffer [2.353 mM $Na_2HPO_4{\cdot}2H_2O$ (Ajax Chemicals) and 17.65 mM KH_2PO_4 (Ajax Chemicals), pH 6.3]. The fluorescence signal per million bacteria was calculated from the density and fluorescence of the bacterial culture used in a particular experiment. The relationship between OD_{600} and the density of the bacterial suspension was determined in a separate calibration curve.

After *Dictyostelium* amoebae were harvested, washed, resuspended at $(1.3–23) \times 10^6$ cells/ml and starved in Sorenson's buffer at 21 °C for 30 min (shaken at 150 rpm) an equal volume of the DsRed-Ec suspension was added. At $t = 0$ and $t = 30$ min 0.5 ml of amoebae were washed free of uningested bacteria by differential centrifugation in the presence of 5 mM sodium azide (Sigma–Aldrich) [34], and the fluorescence was measured in a Modulus fluorometer (Turner Bio-Systems, Sunnyvale, CA) by using a specifically constructed module designed for DsRed (530-nm excitation and 580-nm emission). Measurements were performed in duplicate at each time point. The hourly rate of consumption of bacteria by a single amoeba was calculated from the increase in fluorescence over 30 min, the fluorescence signal per million bacteria and the amoebal density.

2.8. Pinocytosis

For the pinocytosis assay [7,35] axenically growing *Dictyostelium* cells were harvested, resuspended in HL-5 at 2.5–25×10^6 cells/ml, and shaken at 150 rpm for 20 min at 21 °C. The fluorescent compound, Fluoresceinisothiocyanate (FITC)-dextran (Sigma–Aldrich; average mol. mass, 70 kDa; working concentration, 2 mg/ml in HL-5 growth medium) was then added to the cells. At each time point (0 and 60 or 70 min) 200 μl aliquots were transferred to 3 ml of ice-cold phosphate buffer [2 mM $Na_2HPO_4{\cdot}2H_2O$ (Ajax Chemicals) and 15 mM KH_2PO_4 (Ajax Chemicals), pH 6.0). The cells were harvested, washed twice with ice-cold phosphate buffer, and lysed by addition of 2 ml of 0.25% (v/v) Triton X-100 (Sigma–Aldrich) in 100 mM Na_2HPO_4, (Ajax Chemicals), pH 9.2. The fluorescence of the lysate was measured in duplicate at each time point in a Modulus fluorometer (Turner BioSystems) using the Green Module. The rate of uptake of medium per hour, was determined from the cell density, the increase in fluorescence over 60 or 70 min, and a separate calibration curve relating the fluorescence signal to the volume of fluorescent medium.

2.9. Legionella strains and culture

The *L. pneumophila* strains used were derivatives of the pathogenic Corby strain [36]. The *Legionella* was grown on ACES [N-(2-acetamido)-2-aminoethanesulfonic acid] (Sigma–Aldrich)-buffered charcoal yeast extract agar (BCYE) supplemented with 5 μg/ml chloramphenicol (Sigma–Aldrich) at 37 °C with 5% CO_2 for 3 days [37]. For storage the bacteria were frozen in sterile distilled water in 200 μl aliquots and placed at −70 °C. For *Legionella* uptake assays, we used the Corby strain transformed with a plasmid expressing a variant of DsRed, DsRed-Express, which lacks the minor green fluorescence of wild type DsRed [36].

2.10. Infection assay

The intracellular growth of the *L. pneumophila* Corby strain in the *Dictyostelium* cells was quantitated using a growth assay modified from Hägele et al. [24] and Otto et al. [38]. *Dictyostelium* amoebae were grown to a density of $(1–2) \times 10^6$ cells/ml in axenic medium in shaken flasks. Cells were harvested by a 3 min spin at $600 \times g$ and washed twice in Sorensen 1 × C buffer [17 mM KH_2PO_4/Na_2PO_4 (Ajax Chemicals), 50 μM $CaCl_2$ (Ajax Chemicals) pH 6.0] before being finally resuspended in MB medium [0.7% yeast extract (Oxoid Australia), 1.4% proteose peptone (Difco Laboratories), 0.062% $Na_2HPO_4{\cdot}2H_2O$ (Ajax Chemicals), 0.049% KH_2PO_4

(Ajax Chemicals), pH 6.9] at a density of 5×10^5 cells/ml. For each strain 10^5 cells were inoculated into each of 5 wells of a 96-well tissue culture plate. The cells in these wells were used for assaying *Legionella* viable counts at five time points - 0, 24, 48, 72 and 96 h. Cells were allowed to adhere for 30 min at 21 °C prior to being infected with *Legionella*.

L. pneumophila was harvested after growth for 72 h on BCYE plates, resuspended in water and used to infect *D. discoideum* at a MOI of approximately 1:1. The required concentration of bacteria was determined by assuming that OD_{600} of 1 is equivalent to 10^9 bacteria/ml. To initiate infection at the first time point, adherence between *Dictyostelium* and *Legionella* was achieved by centrifuging the bacterial suspension onto the attached amoebae for 10 min at $600 \times g$.

At each assay time point the cells were resuspended, then transferred into a microcentrifuge tube, pelleted for 8 min at $16{,}000 \times g$ in a microcentrifuge and vortexed vigorously for 15 s. A dilution series of the harvested bacteria was then prepared from 10^{-1} to 10^{-4} to measure c.f.u. on BCYE plates incubated at 37 °C with 5% CO_2 for 72–96 h. For the time points ranging from 24 to 96 h the infected amoebae were incubated at 25.5 °C.

2.11. Statistical techniques

Statistical analysis was conducted in the R environment for statistical computing and graphics (http://www.R-project.org).

2.11.1. The Z-test

The proportions of phototaxis mutants were analysed using the *Z* test [39] to determine if the observed frequencies of phototaxis mutants were significantly greater for the tested mitochondrial genes than for nontargeted or chance insertion of "empty" vector into phototaxis loci in the nuclear genome. The significance probability *P* is the probability of occurrence under the null hypothesis of the observed difference between the pho$^-$ mutant proportions for "empty" vector and the test gene constructs.

2.11.2. Exact binomial test

The exact binomial test was used to determine if the expression of mitochondrial genes in the mutants was reduced compared to the parental strain AX2. The significance probability *P* is the probability under the null hypothesis (expression is the same as in AX2 i.e. relative expression equals 1) of the observed proportion of measurements in which the relative expression was less than 1 (i.e. expression less than in AX2)

2.11.3. Analysis of directional data

Individual slugs were analysed for directions of travel using directional statistics based on the circular normal (von Mises) distribution as described previously [18,31]. The accuracy of phototaxis is defined by the concentration parameter (κ) of the circular normal (von Mises) distribution. The κ value indicates how concentrated individual directions are around the mean direction μ (toward the light source). κ ranges from zero when there is no preferred direction of migration to infinity when all directions point exactly toward the light.

2.11.4. Confidence intervals, two sample and multisample tests, correlation analysis

Two sample and multisample tests were performed using one way ANOVA, Kolmogorov–Smirnov, Kruskal–Wallis and Student's *t* tests [39]. Some two sample comparisons and confidence intervals were constructed either by normal Gaussian methods or by bootstrapping using the program *boot.ci* in the *boot* package, in the R environment for statistical computing and graphics (http://www.R-project.org). *Boot.ci* generates nonparametric confidence intervals. The significance of correlations was tested for the Pearson product-moment ρ, the nonparametric Kendall rank correlation coefficient τ, and Spearman rank correlation coefficient ρ.

3. Results

3.1. Isolation of phototaxis-deficient mitochondrial gene disruptants

In all previous studies, mitochondrial dysfunction has resulted in defective phototaxis [10–13,15]. For this reason, in targeted gene disruption experiments we screened all transformants for defects in phototaxis. Examples of the results achieved from these tests are depicted in Fig. 1.

The phototaxis mutant frequencies were analysed statistically to determine if they were significantly higher than the published background level, arising from nontargeted insertion of the "empty vector" pDNeo2 into genes required for normal phototaxis [17]. The results in Table 1 show that in gene disruption experiments targeted at 8 different mitochondrial genes, the frequency of phototaxis mutants amongst the transformants ranged from 1.4% to 12.5% and was significantly greater than in published control transformations using "empty vector" [13]. By contrast, no phototaxis mutants were isolated in control transformations with empty vector, a result consistent with the previously published frequency at which such mutants are isolated by random, nontargeted insertion of this vector into phototaxis genes. The results show that the presence of a mitochondrial gene fragment in the plasmid construct causes its preferential insertion into genes required for normal phototaxis, presumably by homologous recombination into the mitochondrial genome.

For each of the targeted mitochondrial genes, some transformants were retained for further study. Quantitative phototaxis

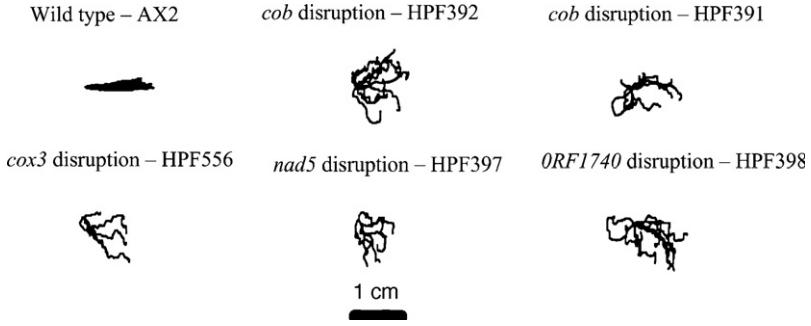

Fig. 1. Qualitative phototaxis of wild type (AX2) and a selection of heteroplasmic mitochondrial gene disruptants. Digitised trails from various strains of *Dictyostelium discoideum* slugs migrating in the presence of a light source positioned at the right of the figure. The wild type strain (AX2) migrated directly towards the light source whereas the mitochondrial gene disruption strains were highly disoriented.

Table 1
Phototaxis and slug migration phenotypes of transformants in targeted disruption experiments.

Targeted gene	No. of transformants	No. Pho$^-$	% Pho$^-$	*Z* statistic	*P* value
cob	165	10	6.06	11.42	<0.01
nad5	156	11	7.05	12.58	<0.01
nad2	90	5	5.56	7.74	<0.01
atp1	24	3	12.50	12.14	<0.01
atp6	146	6	4.11	8.30	<0.01
cox3	270	7	2.59	6.67	<0.01
ORF1740	141	2	1.42	3.17	<0.01
ORF796	75	3	4.00	6.67	<0.01
None	280	0	0	−0.68	0.752
Published background level	3626	6	0.17	NA	NA

The null hypothesis for the *Z*-test was that the frequency of Pho$^-$ mutants derived from targeted disruption experiments was not greater than the expected background in transformations using the empty vector (targeted gene – none). It was tested against the one-sided alternative that Pho$^-$ transformants are isolated at elevated frequencies in the targeted disruption experiments. The *P* value is the probability under the null hypothesis of obtaining at least as many Pho$^-$ transformants as were observed.

Table 2
Effect of heteroplasmic mitochondrial gene disruption on *Dictyostelium* slug phototaxis.

Strain	Targeted mitochondrial gene	Accuracy of phototaxis (κ)	90% confidence intervals	Number of slug trails (sample size)
Wild type (AX2)	None	176	131, 222	79
HPF391	cob	1.97	1.45, 2.50	57
HPF392	cob	0.80	0.497, 1.13	71
HPF397	nad5	2.45	1.70, 3.21	42
HPF559	nad2	2.42	1.60, 3.28	33
HPF560	nad2	1.18	0.742, 1.70	38
HPF563	atp1	2.27	1.59, 2.95	44
HPF557	atp6	2.51	1.73, 3.32	40
HPF553	cox3	1.29	0.94, 1.69	67
HPF565	ORF796	1.84	1.02, 2.83	18
HPF398	ORF1740	1.59	1.21, 2.03	67

The accuracy of phototaxis (κ) is a statistical measure of how concentrated individual directions are around the mean direction towards the light [19]. κ ranges from zero in the case of no preferred direction of migration (all directions equally probable) to infinity in the case of perfect orientation (all directions exactly toward the light).

tests using slugs formed from washed amoebae plated at 2×10^6 cells/ml [18], were performed for these selected mutants (some examples are listed in Table 2). The quantitative data supported the qualitative results in that AX2 migrated towards the light source with high accuracy (κ) whereas the mutants were highly disoriented.

To confirm that plasmid molecules had inserted into the mitochondrial genome of the putative mitochondrial disruptants, a similar method to that used by Wilczynska et al. [13] was employed. Whole genome DNA of each mutant and the parental strain AX2 was prepared, digested with *Bln*I to linearize the circular mitochondrial genome and separated by pulsed field gel electrophoresis (PFGE). Southern blots from the pulsed field gels were probed with α-[^{32}P] dATP-labelled plasmid (pIC19H) DNA. pIC19H shares the same replicon backbone as pDNeo2 which was used for the targeted disruption experiments. A DIG-labelled mitochondrial DNA (mtDNA) probe was also prepared from a mixture of various amplified fragments of the mitochondrial genome. The use of a mixture of probe fragments from various parts of the mitochondrial genome ensured successful detection in Southern blots even in mitochondrial genomes that may have suffered significant deletions. There is evidence in yeast that mitochondrial genome size is regulated [19], so that insertion of exogenous DNA fragments into the *Dictyostelium* mitochondrial genome might have been accompanied by matching deletions elsewhere.

Southern hybridisation analyses with the vector and mtDNA probes revealed the presence of plasmid insertions in the mtDNA band and hence mitochondrial genome disruptions (see Fig. 2 for representative examples). As exhibited in Fig. 2A, signals above the position of the mtDNA band were also evident and these are indicative of chromosomal DNA insertions. This was expected as mitochondrial gene disruptions in such experiments are known to be accompanied by independent, nontargeted insertions into the nuclear genome [13,20]. The plasmid signals associated with the mitochondrial DNA band were weaker than those associated with the chromosomal insertions in the same cells (Fig. 2A). This shows that the number of disrupted mitochondrial genomes was fewer than the number of copies of the construct contained within the individual chromosomal insertions. Previous work in our laboratory has shown that the copy number of constructs within individual chromosomal insertions varies from a few to a few hundred [7,9,11,13,20] and so does not significantly exceed the number of mitochondrial genomes (a few hundred). Accordingly the mitochondrial gene disruptions in our strains must have occurred in only a fraction of the mitochondrial genomes of the cell i.e. the disruptions were heteroplasmic. This was expected because the disruption of every mitochondrial genome in a transformed cell is both improbable and expected to be lethal.

Because of the presence of accompanying insertions into nontargeted chromosomal locations, deleterious phenotypic outcomes in any given transformant could be due to disruption of particular chromosomal genes. However, the insertions into nuclear genes occurred in different locations in every transformant. Therefore, similar patterns of aberrant phenotypes detected amongst the transformants can be ascribed with near certainty to the heteroplasmic mitochondrial genome disruptions. Selected strains that were confirmed to have heteroplasmic mitochondrial gene disruptions of *atp1*, *atp6*, *cob*, *cox3*, *nad2*, *nad5*, *ORF1740* and *ORF796* were tested for a range of phenotypes including multicellular development.

3.2. Multicellular development

Having isolated multiple disruptants for each of the targeted mitochondrial genes, we characterised them phenotypically. Fig. 3 shows representative examples of the morphological defects

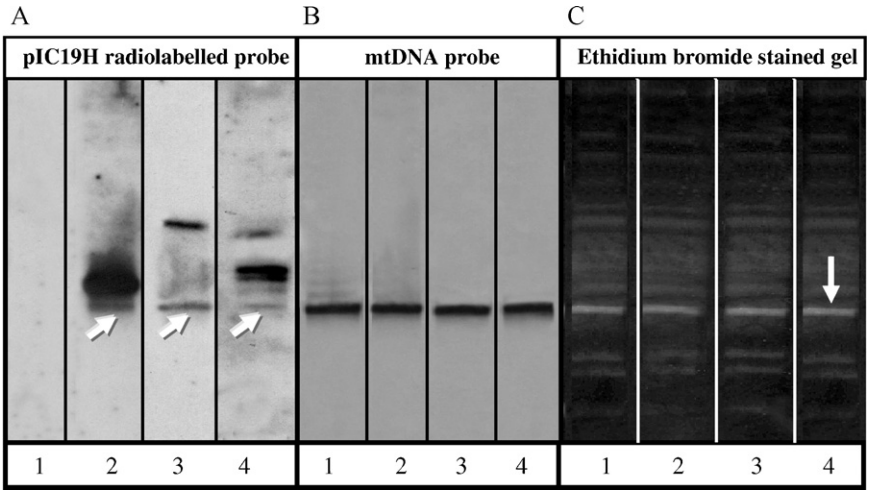

Fig. 2. Pulsed field gel electrophoresis (PFGE) mapping of plasmid insertions in *Dictyostelium* mitochondrial disruptants of wild type strain AX2. Representative results of some mitochondrial targeted disruptants are shown. DNA of whole cell preparations of AX2 and mitochondrial targeted disruptants was digested with *Bln*I, which cuts the mitochondrial genome once. Panel A, Southern blot probed with radioactively-labelled pIC19H revealing the presence of plasmid insertions (arrows) into the mtDNA band. Panel B, Southern blot probed with a DIG-labelled mtDNA probe, showing the position of the mtDNA band (56 kB). Panel C, ethidium bromide stained gel of the whole genome separated by PFGE (the arrow indicates the position of the mtDNA band).

Lane	Strain	Disrupted gene
1	AX2	None
2	HPF392	cob
3	HPF560	nad2
4	HPF397	nad5

observed amongst the mitochondrial gene disruption mutants. Most heteroplasmic mitochondrial gene disruptants formed fewer, undersized fruiting bodies with stalks that were short and thick, along with sori that appeared enlarged relative to the stalks (e.g. Fig. 3A and B), a similar phenotype to that reported for the Cpn60 antisense inhibited strains [7,11]. The sparser, smaller fruiting bodies are indicative of defective aggregation, also exhibited by the *rps4* disruptants [10] and the Cpn60 antisense inhibited strains [11] (Kotsifas et al.). A few strains had such severe dysmorphogenesis that their development ceased after aggregation and consequently these strains only produced mounds (e.g. Fig. 3D). The developmental arrest of these mutants may be a consequence of higher proportions of disrupted mitochondrial genomes, resulting in more severe mitochondrial dysfunction. Bokko et al. [7] noted that in their study, as in that of Kotsifas et al. [11], defects became more evident as the underlying genetic disorder became more severe [6]. This includes arrest at the mound stage of development at the end of aggregation (unpublished results).

3.3. Growth rates

It was previously reported that cell growth and division rates in liquid medium were significantly reduced by mitochondrial dysfunction in *rnl* disruptants [13], *rps4* disruptants [10], Cpn60 antisense-inhibited strains [7,11], *midA* disruptants [12] and mtDNA depleted cells [8]. Generation times during exponential growth were measured (Fig. 4A) and statistical analysis confirmed that the strains with heteroplasmic mitochondrial gene disruptions grew significantly more slowly in liquid medium than AX2. Some mitochondrial gene disruptants (HPF393,569 – *cob* disruptions; HPF565 – *ORF796* disruption; HPF560,561 – *nad2* disruptions) were not able to grow axenically at all, a property which may be considered an extreme form of the slow axenic growth phenotype.

Not only was axenic growth impaired in the mitochondrially diseased strains, but growth on plates with a bacterial food source was also impaired in mitochondrial gene disruptants for all but one of the targeted genes (Fig. 4B). The exception was *ORF1740*, for

Table 3
Details of plasmid constructs and corresponding strains.

Construct name	Gene disrupted	Gene product	Region of gene cloned	DictyBase accession no.	*D. discoideum* mutant strains
pPROF213	atp1	ATPase subunit 1 (ATP synthase F1 alpha)	18–865 bp	DDB0201592	HPF563 and HPF 568
pPROF377	atp6	ATP synthase A chain (protein 6) ATPase subunit 6	205–400 bp	DDB0201600	HPF557
pPROF378	cox3	Cytochrome oxidase subunit 3	499–1265 bp	DDB0201585	HPF553-556
pPROF379	nad2	NADH dehydrogenase subunit 2	297–1183 bp	DDB0201584	HPF559-562
pPROF272	cob	cytochrome b	22874–24043 bp	DDB0201593	HPF391-395 and HPF569
pPROF273	nad5	NADH dehydrogenase subunit 5	399–1281 bp	DDB0201619	HPF396 and HPF397
pPROF274	orf170	Ribosomal protein S3, C-terminal domain-containing protein	1710–2535 bp	DDB0201608	HPF398
pPROF217	orf796	Putative protein of unknown function	46–1468 bp in the *ORF170* sequence	DDB0201617	HPF565 and HPF571

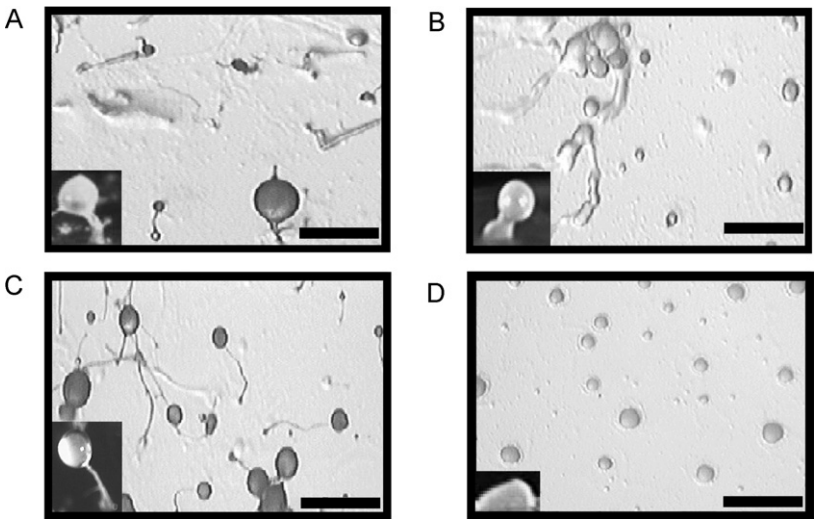

Fig. 3. Effect of heteroplasmic, mitochondrial gene disruption on multicellular morphogenesis. Photographs were taken of morphologies displayed by *Dictyostelium* heteroplasmic mitochondrial gene disruptants grown at 21 °C on *E. coli* B/2. (A) a *nad2* disruptant, HPF561. (B) a *cox3* disruptant, HPF556. (C) wild type (AX2) and (D) a *cob* disruptant, HPF395. The sparse aggregates, short thick stalks and relatively enlarged sori exhibited by HPF561 and HPF556 are typical in the mitochondrial disease strains. In addition to the abnormal fruiting bodies, HPF556 displayed a "broken stream effect" as shown by Panel B of Fig. 3, which may be indicative of defective signal transduction in the aggregation stage. In some strains, such as HPF395, development arrested at the mound stage. The scale bars represent 1 mm.

which the plaque expansion rates were not significantly below wild type. However only one mutant in this class was isolated and tested. Given that the individual mutant strains in any one class of disruptant vary in the degree of severity of the defect and resulting phenotype, it remains possible that disruption in this gene can also cause growth defects on plates. Bokko et al. [7] reported that chaperonin 60 antisense-inhibition also causes slow growth on plates and this was confirmed here using strains isolated by Kotsifas et al. [11] as controls.

3.4. Macropinocytosis and phagocytosis

As the impaired growth of mitochondrially diseased cells could have been due to impaired signal transduction for macropinocytosis or phagocytosis or both, we measured macropinocytosis and phagocytosis rates in AX2 and the mitochondrial disruptants (Fig. 5). All of the mutants exhibited macropinocytosis and phagocytosis rates within or close to the normal range for AX2 (Fig. 5) and no significant impairment of macropinocytosis or phagocytosis was detected statistically for any of the targeted genes (Fig. 6). Phagocytosis and macropinocytosis were also found to be unaltered in mitochondrially diseased cells in which chaperonin 60 expression was antisense inhibited [7].

3.5. Mitochondrially diseased Dictyostelium strains support greater L. pneumophila growth

Dictyostelium has also been used to study the interactions between the intracellular bacterial pathogen *L. pneumophila* and its host [21–27]. When *L. pneumophila* infects host phagocytes, it avoids phagosome-lysosome fusion and subverts host cellular pathways to facilitate its own multiplication inside specialised *Legionella*-containing vesicles (LCVs) within the host cell [28,29].

It was found recently that *Dictyostelium* mitochondria are recruited to *Legionella*-containing vesicles and that mitochondrially diseased *Dictyostelium* cells (mitochondrial dysfunction caused by *rnl* disruption or chaperonin 60 antisense inhibition) were more supportive of *L. pneumophila* growth than healthy cells [9]. We therefore examined whether disruption of the mitochondrial *atp1*, *atp6*, *nad2*, *nad5*, *cox3*, *cob*, *ORF1740* or *ORF796* genes would cause a similar increase in susceptibility to *Legionella*.

Representative results from *Legionella* infection experiments involving mitochondrially diseased cells along with appropriate controls appear in Fig. 6. The *L. pneumophila* viable count increased approximately 50 fold in the presence of wild type *D. discoideum* as host cells. The growth of *L. pneumophila* was dependent upon the presence of *D. discoideum*, since bacteria incubated without the *D. discoideum* host did not grow and instead lost viability over the five-day period. *D. discoideum* in the absence of *L. pneumophila* remained viable throughout the experiment but did not grow under the assay conditions (data not shown). In all classes of mitochondrially diseased strains, the *L. pneumophila* grew significantly faster and reached higher counts than in the parental strain. *L. pneumophila* multiplication was normal in control cells transformed with the empty *Dictyostelium* expression vector, pDNeo2 (HPF226) (data not shown).

3.6. Effect of mitochondrial gene disruption on the expression of mitochondrial genes

The mitochondrial genome in *D. discoideum* is transcribed as a single large polycistronic transcript which is processed by endonucleolytic cleavage to produce mature RNAs [16]. To determine if the heteroplasmic disruption of mitochondrial genes in *D. discoideum* caused a polar or other effect on the expression of downstream genes in the primary transcript, northern hybridisation analyses using gene-specific probes directed at sites near the start, middle and the end of the primary transcript were performed (see Fig. 7A). Fig. 7A shows a map of the *Dictyostelium* mitochondrial genome which indicates the mitochondrial genes disrupted and the position of the probe sequences. The results provided no evidence for a polar effect on expression by any of the gene disruptions and no indication of a dependence of the relative expression levels on the position of the gene targeted for disruption (Fig. 7B). However, compared to AX2 the mitochondrial gene disruptants all exhibited a reduction in expression of genes encoded near the start (*rns*), the middle (*rps13*) and the untranslated end of the primary mitochondrial RNA transcript. We conclude that heteroplasmic disruption of mitochondrial genes

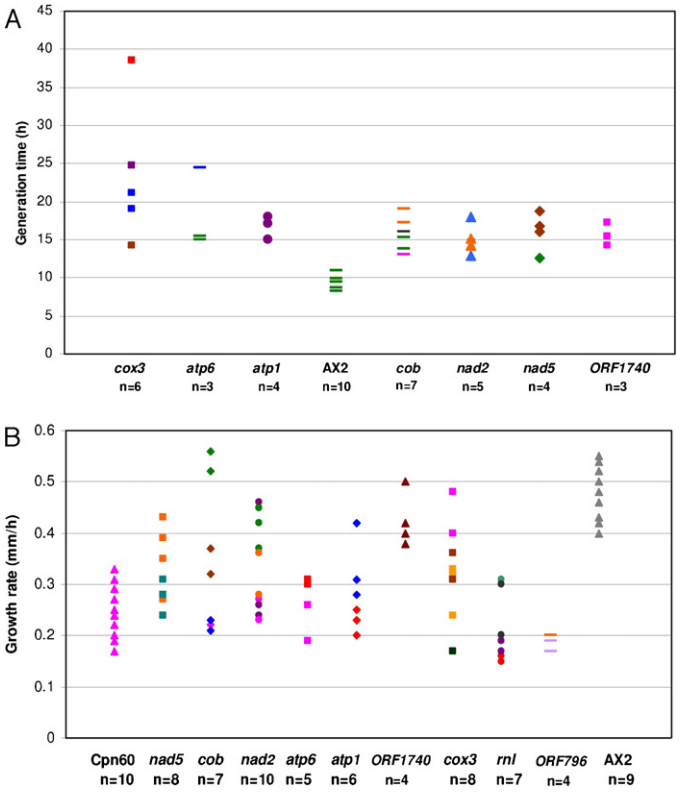

Fig. 4. Heteroplasmic mitochondrial gene disruption causes slow growth. The mitochondrial gene targeted for heteroplasmic disruption appears along the *x* axis. AX2 is the wild type parental strain and the other strains that appear are mutants. Sample sizes (*n*, the number of independent growth experiments on mutant strains) for each class of mutant are indicated below each gene name. Different coloured data points for each mutant class represent specific strains. In the case of AX2, the sample size is the number of independent growth experiments. In some cases the indicated value of "*n*" may be higher than the total number of visible points because some data points overlap. (A). Generation times. The generation times refer to the doubling time during exponential growth in HL-5 medium shaken at 150 rpm at 21 °C. The generation times for the mitochondrially diseased strains were significantly longer than AX2 according to the results of Kolmogorov–Smirnov, Kruskal–Wallis and Student's *t* two-sample (unequal variance) tests at $p < 0.05$ or < 0.01. (B) Plaque expansion rates during growth on *E. coli* B2 lawns. The strains tested included mitochondrially diseased transformants that have either heteroplasmic mitochondrial gene disruptions or antisense inhibition of Cpn60 (chaperonin 60). The growth rates for the mitochondrially diseased strains (except for the *ORF1740* disruptants) were significantly lower than AX2 according to the results of Kolmogorov–Smirnov, Kruskal–Wallis and Student's *t* two-sample (unequal variance) tests ($p < 0.05$).

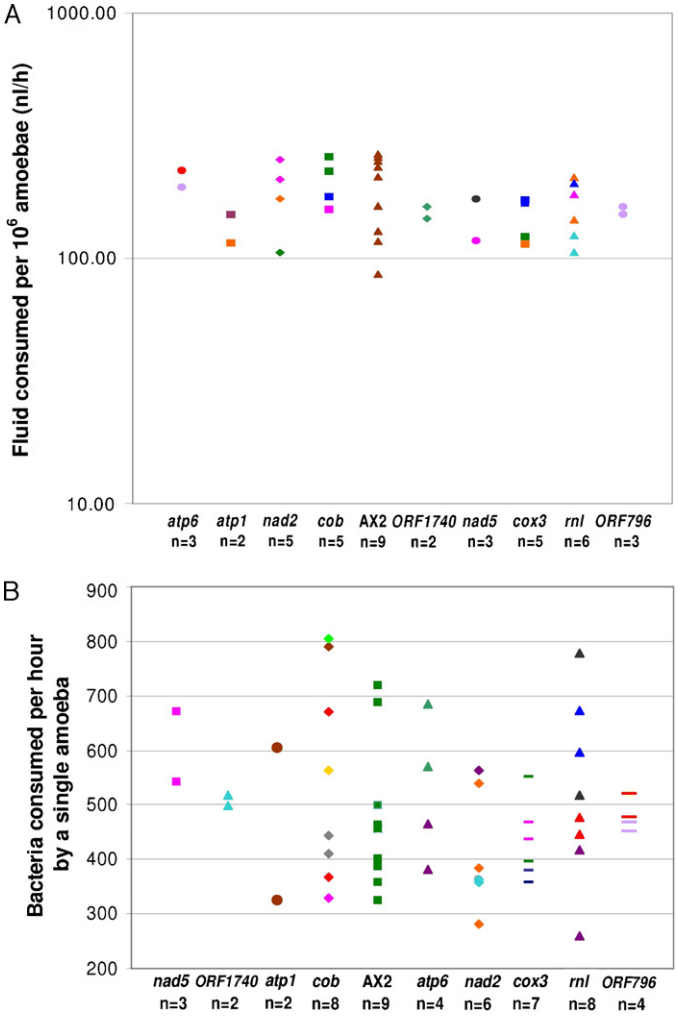

Fig. 5. Heteroplasmic mitochondrial gene disruption does not affect endocytosis rates. The mitochondrial gene targeted for disruption is indicated on the *X* axis. Sample sizes (*n*, the number of independent growth experiments on mutant strains) for each class of mutant are indicated below each gene name. Different coloured points for each mutant class represent specific strains. In some cases the indicated value of "*n*" may be higher than the total number of visible points because some data points overlap. (A) Macropinocytosis. The rate of uptake of fluorescent medium containing 2 mg/mL FITC dextran was measured. The rates for the mitochondrially diseased strains were not significantly different from those for AX2 in Kolmogorov–Smirnov, Kruskal–Wallis and Student's *t* two-sample (unequal variance) tests ($p > 0.05$). (B) Phagocytosis. Rates of phagocytosis are shown for *Dictyostelium* cells that have engulfed *E. coli* cells expressing the fluorescent red protein, Ds-Red. The rates for the mitochondrially diseased strains were not significantly different from those for AX2 in Kolmogorov–Smirnov, Kruskal–Wallis and Student's *t* two-sample (unequal variance) tests ($p > 0.05$).

causes a general reduction in mitochondrial gene expression, regardless of the location of the disrupted gene. This would be expected to produce a general, sublethal mitochondrial dysfunction and is consistent with the phenotypic patterns observed in the mutants.

4. Discussion

The symptoms associated with human mitochondrial diseases are extremely variable and are not tightly coupled to genotype. Mitochondrial disease in *Dictyostelium* was first created by disrupting the mitochondrial large ribosomal subunit RNA gene (*rnl*) in a subset of the mitochondria [13]. The aberrant phenotypes resulting from this heteroplasmic gene disruption were similar to those observed as a result of antisense inhibiting expression of the nuclear-encoded mitochondrial chaperone, chaperonin 60 [11]. This suggests that phenotype–genotype relationships are more regular in this simple mitochondrial disease model and offers the opportunity to determine if the cytopathological outcomes are similar regardless of which mitochondrial gene is targeted for disruption.

To test this we studied the phenotypic outcomes in mutant strains, in each of which a mitochondrial gene had been targeted for disruption. Some of the mitochondrial genes targeted for disruption are required while others are not known to be essential for mitochondrial energy production. We successfully generated heteroplasmic mitochondrial genome disruptions in *D. discoideum* in experiments that targeted eight different mitochondrial genes scattered throughout the mitochondrial genome.

A range of phenotypes were examined in the mutants and a consistent pattern of phenotypic outcomes was observed amongst the mitochondrially diseased strains regardless of whether the product encoded by the targeted gene was known to be essential for

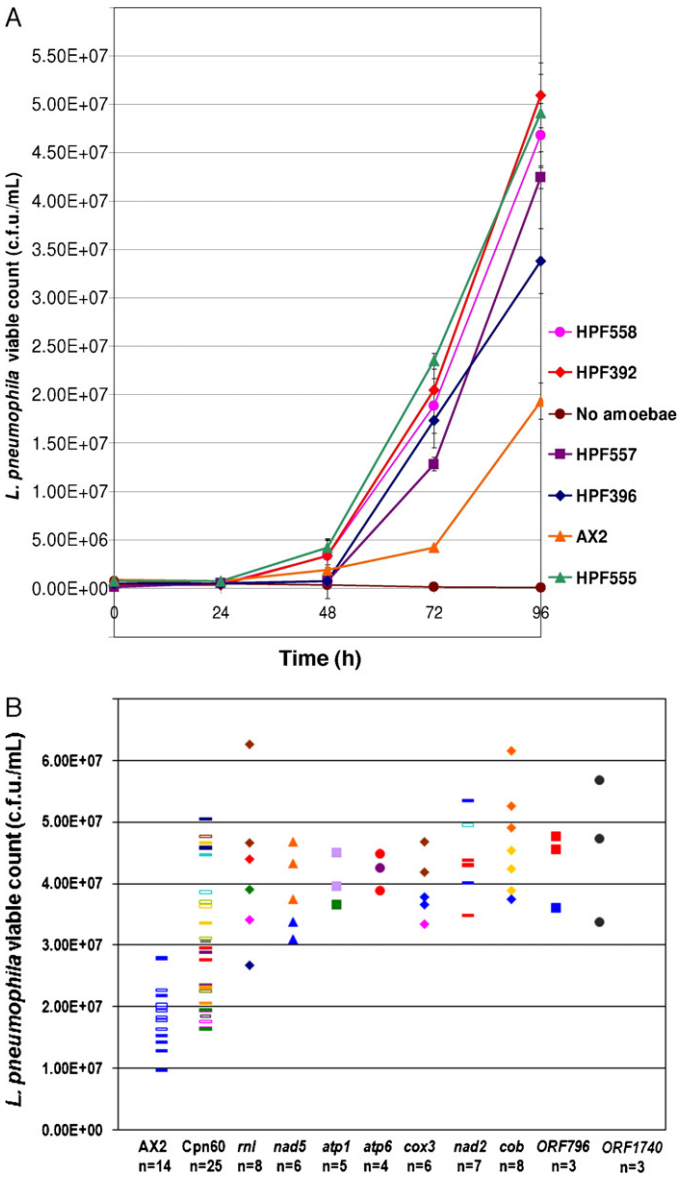

Fig. 6. Mitochondrial disease enhances susceptibility to *Legionella* in *Dictyostelium*. The cells of all strains were infected with the *L. pneumophila* Corby strain over a 96 h period. The wild type (AX2) strain was used as a control. A negative control in which the *Legionella* were plated with no host amoebae was also included. (A) Bacterial viable counts are plotted as a function of time. Viable counts were performed in duplicate or triplicate. Error bars are standard errors reflecting viable count errors within the experiment. The strains with mitochondrial dysfunction carry heteroplasmic mitochondrial gene disruptions of *nad2* (HPF558), *nad5* (HPF396), *cob* (HPF392), *atp6* (HPF557) and *cox3* (HPF555). (B) *Legionella* viable counts on the 5th day (after 96 h) of infection of normal (AX2) or mitochondrially diseased cells. Each point represents a separate experiment and each different symbol indicates a different, independent mutant. The *X* axis indicates the mutant class – either chaperonin 60 antisense inhibition (Cpn60) or the mitochondrial gene targeted for disruption. Chaperonin 60 antisense inhibition (Cpn60) and *rnl* disruption strains are included as positive controls, since strains in these classes have been reported previously to support greater intracellular *Legionella* proliferation [9]. The extent of *Legionella* proliferation in the mitochondrially diseased strains was significantly greater than in AX2 according to the results of Kolmogorov–Smirnov, Kruskal–Wallis and Student's *t* two-sample (unequal variance) tests ($p < 0.05$).

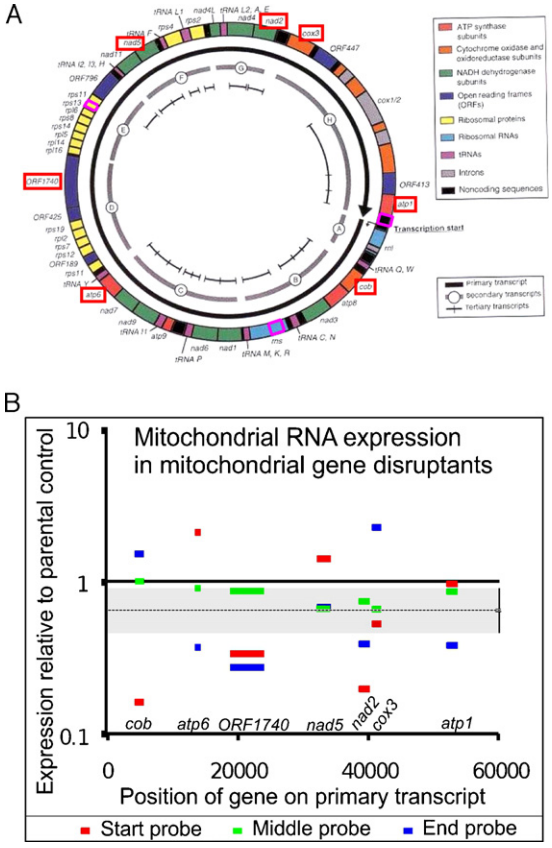

Fig. 7. Expression of the mitochondrial genome is reduced in mitochondrial gene disruptants. (A). Map of the *Dictyostelium discoideum* mitochondrial genome. This map indicates the 7 targeted genes (red boxes) in mutants used in the expression experiments and the areas of the mitochondrial genome that were amplified via PCR to create mitochondrial DNA probes (pink boxes). Figure adapted from Barth et al. [6]. (B). Mitochondrial RNA expression in mitochondrial disruptants. Mitochondrial RNA expression levels were measured in quantitative northern blots, normalized against total RNA and calculated relative to the expression level in the parental strain AX2. Expression levels in 7 different disruptant strains using each of 3 different probes is plotted against the position of the disrupted gene in the mitochondrial primary transcript. Red, green and blue symbols/lines indicate the relative expression levels assayed using probes for sequences located respectively near the start (at nucleotides 7187–8209, in *rns*), middle (at nucleotides 26710–27180, in *rps13*) and end (at nucleotides 53716–55510, in untranslated sequence) of the primary transcript. For each mutant strain, the symbol/line is plotted at the position of the gene targeted for disruption in that strain and the name of the targeted gene is indicated on the *X* axis. There was no correlation between the level of expression detected by any of the three probes and the position of the targeted gene (Pearson, Spearman and Kendall correlation coefficients). Analysis of variance and multisample Kruskal–Wallace tests showed that there were no significant differences in relative expression levels amongst the three probed sequences. The dotted line represents the geometric mean (0.66) of relative expression levels averaged over all three probed sequences in all 7 disruptant strains and the 95% confidence intervals for it are represented by the grey area and the error bars on the right boundary of the grey area. These and the exact binomial test ($P < 0.01$) showed that the relative expression levels in the mutant strains were significantly less than 1 (i.e. less than the parental wild type strain AX2).

oxidative phosphorylation (OXPHOS). These phenotypic consequences of heteroplasmic mitochondrial gene disruption included slow growth on plates and in liquid medium, impaired phototaxis, aberrant multicellular development and increased susceptibility to the intracellular bacterial pathogen *L. pneumophila*. Processes found to be unaffected by heteroplasmic mitochondrial gene disruption were phagocytosis and macropinocytosis. This pattern of phenotypic outcomes is similar to that caused by antisense inhibition of chaperonin 60 expression or by heteroplasmic disruption of the mitochondrial *rnl* gene [7,9,11].

The regularity of the mitochondrial disease phenotypes in *Dictyostelium* suggests that regardless of the genetic cause, a common cytopathological mechanism underlies the resulting disease. In humans, where the clinical outcome of mitochondrial disease is extremely diverse, such a common underlying cytopathological process may be obscured by individual, age-related and tissue-specific differences in the severity of the underlying

genetic disorder and the energy requirements of the cells [40]. What might this underlying mechanism be? Based on experiments in the *Dictyostelium* model, Bokko et al. [7] and Francione et al. [9] suggested that diverse phenotypic outcomes of mitochondrial disease result from dysregulated signalling caused by chronic hyperactivity of the conserved, energy-sensing protein kinase AMPK (AMP-activated protein kinase).

Despite the consistent phenotypic outcomes caused by chaperonin 60 knock down, or heteroplasmic disruption of mitochondrial genes, variant patterns of phenotypes have also been observed. In particular, knockout of *midA*, a chromosomal gene encoding a conserved mitochondrial protein, causes defects in phagocytosis and pinocytosis that have not been observed in other mutants [12]. The MidA protein is specifically required for the expression and function of Complex I, the first of the multisubunit enzymes in the mitochondrial electron transport chain [15]. In our heteroplasmic gene disruption experiments, neither phagocytosis nor pinocytosis was affected by specifically targeting either of two mitochondrially encoded subunits (*nad5*, *nad2*) of Complex I. Instead these mutants exhibited the same aberrant phenotypes as are caused by chaperonin 60 knock down or targeted disruption of other mitochondrial genes including *rnl*. This suggests that the phenotypes we observe are caused by a general mitochondrial dysfunction and are not specific consequences of disrupting specific genes.

In support of such a general impairment of mitochondrial function we observed reduced levels of mitochondrial genome expression in our mutants in quantitative northern blots. There are at least two possible mechanisms by which this could occur. Firstly, in our experiments and in the previously reported *rnl* disruptions [13], the size of the mitochondrial genome (56 kb) in pulsed field gels was not noticeably changed by the insertion. This is consistent with the observation in yeast that mitochondrial genome size is regulated [19]. It suggests the possibility that in our mutants the insertions are accompanied by large mitochondrial genome deletions which could contribute to reductions in expression of other mitochondrial genes. Secondly, the mitochondrial genome in *Dictyostelium* is transcribed from a single unidirectional promoter and the resulting transcript is processed to produce all of the smaller functional RNA molecules in the mitochondria [16]. This arrangement lends itself to coordinate regulation of mitochondrial gene expression and raises the possibility that plasmid insertions in the mitochondrial genome interfere with the transcription, the processing or the stability of the primary mitochondrial RNA transcript. Regardless of the mechanism, our mutants exhibited a depression in the steady state levels of three representative mitochondrial RNAs derived from near the start, middle and end of the full length primary transcript. The result would be a coordinate, general impairment of mitochondrial function.

By contrast, the MidA knockout specifically reduces the level and activity of Complex I while the levels and activities of the other respiratory chain complexes actually increase [15]. The MidA knockout strain thereby revealed a compensatory feedback process that responds to mitochondrial dysfunction by increasing the levels of the respiratory chain complexes but specifically fails in the case of Complex I. Carilla-Latorre et al. [15] suggested that phagocytosis and pinocytosis are specifically impaired either by the reduced activity of Complex I or by the absence of MidA itself, producing in turn an AMPK-independent impairment of growth on bacteria and in liquid medium. The MidA mutant also exhibited an AMPK-dependent impairment of phototaxis and thermotaxis, showing that AMPK is chronically activated also in the case of a specific Complex I deficiency. We conclude that coordinate reductions in mitochondrial function, such as observed in our mutants, produce AMPK-dependent cytopathology. On the other hand, specific defects in particular proteins (such as MidA) can produce additional, specific cytopathologies that are superimposed upon the AMPK-mediated defects.

Conflict of interest

The authors declare that there are no conflicts of interest.

Acknowledgements

L.F. was a recipient of an Australian Postgraduate Research Scholarship. This work was supported by grants from the Thyne Reid Memorial Trusts and the Australian Research Council. We are grateful to Dr. Sarah Annesley for helpful comments on the manuscript.

References

[1] Francione L, Fisher PR. Cytopathological mechanisms in mitochondrial disease. Curr Chem Biol 2010;4:32–48.
[2] McKenzie M, Liolista D, Hanna MG. Mitochondrial disease: mutations and mechanisms. Neurochem Res 2004;29:589–600.
[3] Zeviani M, Carelli V. Mitochondrial disorders. Curr Opin Neurol 2007;20: 564–71.
[4] Rossignol R, Faustin B, Rocher C, Malgat M, Mazat J, Letellier. Mitochondrial threshold effects. Biochem J 2003;370:751–62.
[5] Francione LM, Annesley SJ, Carilla-Latorre S, Escalante R, Fisher PR. The *Dictyostelium* model for mitochondrial disease. Semin Cell Dev Biol 2011;22:120–30.
[6] Barth C, Le P, Fisher PR. Mitochondrial biology and disease in *Dictyostelium*. Int Rev Cytol 2007;263:207–52.
[7] Bokko PB, Francione L, Bandala-Sanchez E, Ahmed AU, Annesley SJ, Huang X, et al. Diverse pathologies in mitochondrial disease are caused by AMP-activated protein kinase signalling. Mol Biol Cell 2007;18:1874–86.
[8] Chida J, Yamaguchi H, Amagai A, Maeda Y. The necessity of mitochondrial genome DNA for normal development of *Dictyostelium* cells. J Cell Sci 2004;117:3141–52.
[9] Francione L, Smith PK, Accari SL, Taylor PE, Bokko PB, Bozzaro S, et al. *Legionella pneumophila* multiplication is enhanced by chronic AMPK signalling in mitochondrially diseased *Dictyostelium* cells. Dis Model Mech 2009;2:479–89.
[10] Inazu Y, Chae SC, Maeda Y. Transient expression of a mitochondrial gene cluster including *rps4* is essential for the phase-shift of *Dictyostelium* cells from growth to differentiation. Dev Genet 1999;25:339–52.
[11] Kotsifas M, Barth C, Lay ST, de Lozanne A, Fisher PR. Chaperonin 60 and mitochondrial disease in *Dictyostelium*. J Muscle Res Cell Motil 2002;23: 839–52.
[12] Torija P, Vicente JJ, Rodrigues T, Robles A, Cerdan S, Sastre L, et al. Functional genomics in *Dictyostelium*: MidA, a new conserved protein, *is required* for mitochondrial function and development. J Cell Sci 2006;119:1154–64.
[13] Wilczynska Z, Barth C, Fisher PR. Mitochondrial mutations impair signal transduction in *Dictyostelium discoideum* slugs. Biochem Biophys Res Commun 1997;234:39–43.
[14] Ogawa S, Yoshino R, Angata K, Iwamoto M, Pi M, Kuroe K, et al. The mitochondrial DNA of *Dictyostelium discoideum*: complete sequence, gene content and genome organisation. Mol Gen Genet 2000;263:514–9.
[15] Carilla-Latorre S, Gallardo ME, Annesley SJ, Calvo-Garrido J, Graña O, Accari SL, et al. MidA is a putative methyltransferase required for mitochondrial complex I function. J Cell Sci 2010;123:1674–83.
[16] Le P, Fisher PR, Barth C. Transcription of the *Dictyostelium* genome occurs from a single initiation site. RNA 2009;15:2321–30.
[17] Wilczynska Z, Fisher PR. Analysis of a complex plasmid insertion in a phototaxis-deficient transformant of *Dictyostelium discoideum* selected on a *Micrococcus luteus* lawn. Plasmid 1994;32:182–94.
[18] Fisher PR, Annesley SJ. Slug phototaxis, thermotaxis and spontaneous turning behaviour. In: *Dictyostelium discoideum* Protocols. Methods in Molecular Biology. NJ: Humana Press; 2006. p. 137–70.
[19] Thorsness PE, Fox TD. Escape of DNA from mitochondria to the nucleus in *Saccharomyces cerevisiae*. Nature 1990;346:376–9.
[20] Barth C, Fraser DJ, Fisher PR. Coinsertional replication is reponsible for tandem multimer formation during plasmid integration into the *Dictyostelium* genome. Plasmid 1998;39:141–53.
[21] Eichinger L, Lee SS, Schleicher M. *Dictyostelium* as a model system for studies of the actin cytoskeleton by molecular genetics. Microsc Res Tech 1999;47: 124–34.
[22] Fajardo M, Schleicher M, Noegel A, Bozzaro S, Killinger S, Heuner K, et al. Calnexin, calreticulin and cytoskeleton-associated proteins modulate uptake and growth of *Legionella pneumophila* in *Dictyostelium discoideum*. Microbiology 2004;150:2825–35.
[23] Farbrother P, Wagner C, Na J, Tunggal B, Morio T, Urushihara H, et al. *Dictyostelium* transcriptional host cell response upon infection with *Legionella*. Cell Microbiol 2006;8:438–56.

[24] Hägele S, Köhler R, Merkert H, Schleicher M, Hacker J, Steinert M. *Dictyostelium discoideum*: a new host model system for intracellular pathogens of the genus *Legionella*. Cell Microbiol 2000;2:165–71.
[25] Peracino B, Wagner C, Balest A, Balbo A, Pergolizzi B, Noegel A. Function and mechanism of action of *Dictyostelium* Nramp1 (Slc11a1) in bacterial infection. Traffic 2006;7:22–38.
[26] Skriwan C, Fajardo M, Hägele S, Horn M, Wagner M, Michel R, et al. Various bacterial pathogens and symbionts infect the amoeba *Dictyostelium discoideum*. Int J Med Microbiol 2002;291:615–24.
[27] Soloman JM, Rupper A, Cardelli JA, Isberg RR. Intracellular growth of *Legionella pneumophila* in *Dictyostelium discoideum*, a system for genetic analysis of host-pathogen interactions. Infect Immun 2000;68:2939–47.
[28] Horwitz MA. Legionnaires' disease bacterium (*Legionella pneumophila*) inhibits phagosome-lysosome fusion in human monocytes. J Exp Med 1983;158:2108–26.
[29] Horwitz MA, Silverstein SC. Legionnaires' disease bacterium (*Legionella pneumophila*) multiplies intracellularly in human monocytes. J Clin Investig 1980;66:441–50.
[30] Watts DJ, Ashworth JM. Growth of myxameobae of the cellular slime mould *Dictyostelium discoideum* in axenic culture. Biochem J 1970;119: 171–4.
[31] Fisher PR, Smith E, Williams KL. An extracellular chemical signal controlling phototactic behaviour by *D. discoideum* slugs. Cell 1981;23:799–807.
[32] Cox EC, Vocke CD, Walter S, Gregg KY, Bain ES. Electrophoretic karyotype for *Dictyostelium discoideum*. Proc Natl Acad Sci USA 1990;87:8247–51.
[33] Chu G, Vollrath D, Davis RW. Separation of large DNA molecules by contour-clamped homogenous electric fields. Science 1986;234:1582–5.
[34] Maselli A, Laevsky G, Knecht DA. Kinetics of binding, uptake and degradation of live fluorescent (DsRed) bacteria by *Dictyostelium discoideum*. Microbiology 2002;148:413–20.
[35] Klein G, Satre M. Kinetics of fluid-phase pinocytosis in *Dictyostelium discoideum* amoebae. Biochem Biophys Res Commun 1986;138:1146–52.
[36] Mampel J, Spirig T, Weber SS, Haagensen JAJ, Molin S, Hilbi H. Planktonic replication is essential for biofilm formation by *Legionella pneumophila* in a complex medium under static and dynamic flow conditions. Appl Environ Microbiol 2006;72:2885–95.
[37] Wintermeyer E, Ludwig B, Steinert M, Schmidt B, Fischer G, Hacker J. Influence of site specifically altered Mip proteins on intracellular survival of *Legionella pneumophila* in eukaryotic cells. Infect Immun 1995;63:4576–83.
[38] Otto GP, Wu MY, Kazgan N, Anderson OR, Kessin RH. *Dictyostelium* macroautophagy mutants vary in the severity of their developmental defects. J Biol Chem 2004;279:15621.
[39] Siegel S. Nonparametric Statistics for the Behavioural Sciences. Tokyo: Kogalaisha-Ltd; 1956.
[40] McFarland R, Turnbull DM. Batteries not included: diagnosis and management of mitochondrial disease. J Int Med 2009;265:210–28.